

Investigation of Hydrogen Storage Using Combinatorial Thin Films and IR Imaging

Hiroyuki Oguchi¹, Ichiro Takeuchi¹, Daniel Josell², Edwin J Heilweil², and Leonid A Bendersky²

¹University of Maryland, College Park, MD, 20742

²National Institute of Standards and Technology, Gaithersburg, MD, 20899

ABSTRACT

Three 100 nm-thick $Mg_x(TM)_{1-x}$ (TM = Ni and Ti) composition-spread thin films having compositional variation $0.4 < x < 0.95$ and capped with a 5 nm-thick Pd layer were deposited in combinatorial electron-beam deposition chamber. The crystallinity of the films was characterized by scanning x-ray diffraction and cross-sectional transmission electron microscopy. Hydrogen absorption and desorption of the films were monitored with an infrared camera capable of simultaneously imaging the entire composition spread. The observed changes in infrared intensity due to hydrogen absorption/desorption demonstrate the sensitivity of the method to the differences in composition, microstructure and type of TM.

INTRODUCTION

Discovering new lightweight hydrogen storage materials is essential for the practical use of hydrogen as an alternative fuel for transportation [1,2]. High-throughput screening of combinatorial samples to identify high capacity hydrogen storage materials with fast absorption and desorption kinetics can be of great importance to accelerate the discovery of such materials. Surprisingly, combinatorial methods have not been widely applied to the problem of multi-component metal hydride discovery. A notable exception is systematic and comprehensive study of thin films via optical methods (coined “hydrogenography”) introduced by Prof. Griessen’s et. al. [3, 4]. This method relies on dramatic changes in optical transparency of films as a response to hydrogen absorption.

In this paper we report a complementary technique to the optical method of observing hydrogenation of combinatorial thin films – infrared (IR) imaging. Similar to the optical changes, IR emissivity of a solid is expected to change with hydrogen adsorption as a result of changes in its electronic and vibrational energy states, as well as its crystallographic structure. Application of IR imaging to hydrogenation studies was reported recently by General Electric and General Motors researchers [5,6]. The main goal of the paper is to demonstrate the feasibility of the application of in-situ IR imaging method to Mg-transition metals composition-spread thin films.

In this study we investigated the hydrogenation of electron-beam (e-beam) deposited Mg_xNi_{1-x} and Mg_xTi_{1-x} ($0.95 > x > 0.4$) compositional gradient thin films capped with 5 nm-thick Pd layer; capping films with Pd is known to prevent oxidization of films and catalyze hydrogenation reaction [3, 4]. The composition of the studied films was selected for two reasons: First, Mg-based alloys are of great interest for hydrogen storage research due to the high gravimetric density of hydrogen in MgH_2 ; the improvement of thermodynamics and kinetics through alloying and structural modification has been studied intensively [7,8]. Second, hydrogenation of Mg_xNi_{1-x} [10, 11] and Mg_xTi_{1-x} [13] films was extensively studied recently by optical method for their mirror switching properties. These studies showed that hydrogenation of the films occurs at temperatures and pressures much lower than needed for bulk alloys and exhibit improved kinetics. Although the hydrogenation properties can be sensitive to particular

film preparation condition and method, the published results provide good references for our measurements.

EXPERIMENTAL

Two $\text{Mg}_x\text{Ni}_{1-x}$, and one $\text{Mg}_x\text{Ti}_{1-x}$ composition spread thin films were deposited on thermally oxidized Si(100) substrates using the multilayer-deposition technique in a combinatorial e-beam deposition chamber. In this technique, after one cycle of shadow mask motion, a unit layer, which itself is composed of wedge-like sub-layers, with average composition continuously varying along a substrate is deposited. The cycles are repeated hundreds of times, until a film of suitable thickness has been deposited. The thickness of the wedge-like sub-layer is a key factor in realizing complete mixing of the layers; it was determined via cross-sectional transmission electron microscopy (TEM) that for Mg-TM (TM – transition metals) systems atomic-scale mixing can be achieved with 0.5 nm-thick unit layers. All composition spreads were capped with a 5 nm-thick Pd layer.

To study the effect of microstructural differences on hydrogen absorption/desorption, one $\text{Mg}_x\text{Ni}_{1-x}$ film was annealed in the deposition chamber at 250 °C for 2 hours after being deposited. The composition spreads were capped with Pd after post-annealing to prevent the formation of undesirable phases at the interface. Typical dimension of the sample is 13 mm (length) x 8 mm (width) x 100 nm (thickness). The composition and crystallinity of the thin films were measured along the composition gradient using energy dispersive spectroscopy (EDS) and scanning x-ray diffraction (XRD) with area detector, respectively.

Hydrogen absorption/desorption of the films was studied by acquiring IR images in-situ during hydrogenation of the samples. The samples were set in a hydrogenation chamber, clamped to a heating stage, and IR emission images were continuously collected every 30 sec through a sapphire window. The employed IR camera array is composed of a 256x256 array of InSb diodes, which are electrically biased to permit “snap-shot” imaging (with 10 microsecond or longer integration times). The camera has its peak sensitivity at a wavelength of 5 micrometers, but it is able to detect over an integrated range of 1.0 to 5.5 microns to increase total intensity. The IR emission images were analyzed post acquisition through image analysis software to extract the temporal evolution of each intensity pixel (evolution of IR intensity for a selected composition). Normalized IR intensities (IR intensity of the thin films divided by IR intensity of from a fixed region of the Si substrate) were plotted as a function of measurement time (and hydrogenation conditions) for 30 measurement points along the composition gradient.

RESULTS

Composition of the films.

Composition variations of the studied films are shown in Fig. 1.

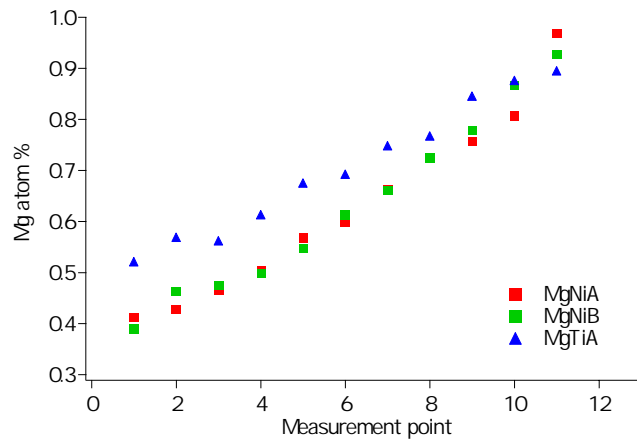


Fig. 1 Composition variation of Mg_xNi_{1-x} (red and green squares) and Mg_xTi_{1-x} (blue triangles) films measured by EDS along the composition spread direction every 0.1 cm.

The measurement points along a composition gradient are taken every 0.1 cm across the entire spread. All samples show near-linear variation of composition ($0.4 < x < 0.95$ for Mg_xNi_{1-x} and $0.5 < x < 0.9$ for Mg_xTi_{1-x}), with good run-to-run reproducibility.

Crystallinity of the films.

Crystallinity of the films was studied using scanning XRD. For each sample, 10 equally spaced measurement points encompassing the entire composition gradient were chosen. Obtained θ -2 θ XRD scans are shown in Fig. 2(a-c). Each figure consists of 10 scans taken from the 10 measurement points of different compositions. The scans are offset to show results for multiple compositions, with upper scans having the highest Mg composition. Si(400) peak from a substrate and Pd(111) peak are seen at 69.1° and 40.1° , respectively, for all the samples.

XRD scans of the as-deposited Mg_xNi_{1-x} (Fig. 2(a)) don't show any peaks from the Mg or Ni phases, thus suggesting the entire composition spread is either amorphous or nano-crystalline. TEM studies are in progress to resolve the details of the microstructures. According to recent publications on Mg_xNi_{1-x} films, for different deposition methods, conditions, and substrates the Mg_xNi_{1-x} films can be either crystalline [9] or x-ray amorphous [10].

XRD scans of the 250 °C-annealed Mg_xNi_{1-x} film, Fig. 2b, show the appearance a new peak at 44° for the composition range of $x=0.4-0.5$. The peak is consistent with the (114) of $MgNi_2$. The difference in the XRD patterns for the two Mg_xNi_{1-x} films suggests that structural modification was achieved by 250 °C post-annealing, which is expected to affect hydrogenation.

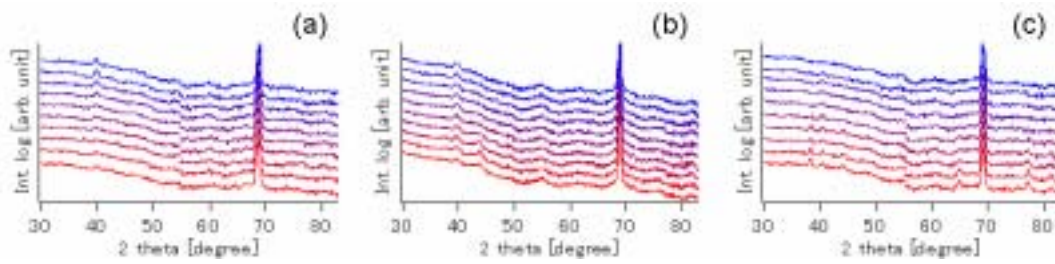


Fig. 2 XRD patterns of as-deposited Mg_xNi_{1-x} (a), annealed Mg_xNi_{1-x} (b), and as-deposited Mg_xTi_{1-x} (c). Each figure consists of 10 scans, which corresponds to 10 measurement points with different compositions. The scans are vertically offset, with highest Mg composition on top.

Fig. 2(c) shows XRD scans from the Mg_xTi_{1-x} as-deposited film. No peaks (with the exception of Si and Pd) are detected for the composition range ($0.9 > x > 0.7$). Ti(002), Ti(201), and Ti(004) peaks are observed at around 38.2° , 77.1° , and 81.4° , respectively, for the lower Mg composition range of $0.7 > x > 0.5$. In addition, two unidentified peaks were observed at around 44.2° and 64.9° for the same range of 0.5 - 0.7 Mg. Since intensity of these peaks monotonously decreases with decreasing Ti composition, we suspect the presence of an unknown MgTi compound. Note that there are no equilibrium MgTi intermetallic compounds according to the phase diagram [13]; therefore the unknown phase is either metastable MgTi or a product of an interfacial reaction. The XRD results for Mg_xTi_{1-x} are different from those reported in literature where for higher Mg compositions the peaks of Mg(Ti) solid-solution phase were seen [11,12]. The differences are probably reflecting the differences in deposition processes, and TEM work is in progress to identify the unknown phase and the reasons for the absence of Mg peaks.

Hydrogenation experiments and IR measurements.

Evolution of normalized IR intensities with time during hydrogenation experiments are shown for Mg_xNi_{1-x} as-deposited, Mg_xNi_{1-x} annealed, and Mg_xTi_{1-x} films in Fig. 3(a), (b), and (c), respectively. In these experiments the films were initially equilibrated at 150°C prior to exposing the samples to hydrogen, thus the change in the film's IR emissivity during hydrogenation could be attributed only to the changes in the amount of hydrogen in a film. Equally spaced 30 measurement points along composition spreads are selected in the acquired IR images. The offsetted curves in Fig. 3 show evolution of IR intensity with time for these selected compositions. Top of each figure shows conditions of the hydrogenation experiments: hydrogen pressure P_H (bar) and film's temperature T_S ($^\circ\text{C}$).

For the as-deposited Mg_xNi_{1-x} , Fig. 3(a), IR intensity for the compositions $x > 0.5$ was increasing immediately after pressurizing the sample with 1 bar hydrogen gas at 150°C (1 - 2 h); however the change was small for the compositions $x < 0.5$. The rate of intensity increase is higher for the higher Mg compositions.

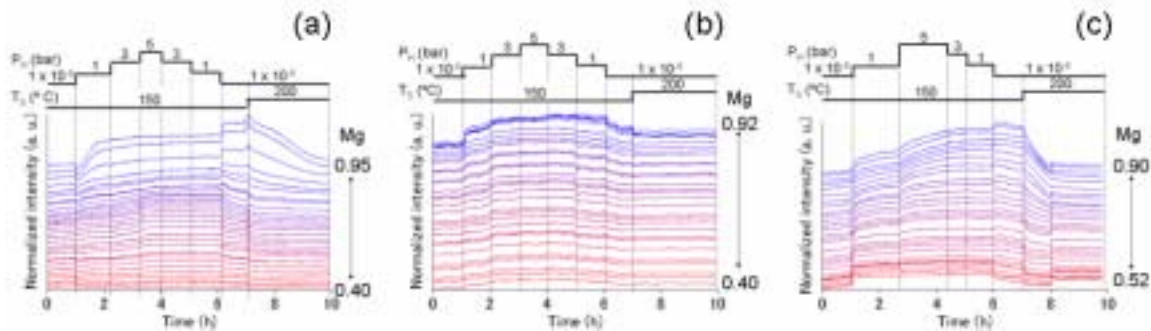


Fig. 3 Normalized IR intensity of as-deposited Mg_xNi_{1-x} (a), annealed Mg_xNi_{1-x} (b), and as-deposited Mg_xTi_{1-x} (c). Equally spaced 30 measurement points along composition spread are chosen from one edge to another edge for each sample. By applying vertical offset, 30 normalized IR intensity curves as a function of measurement time are aligned to show you results of more Mg atomic % points at higher location on each figure. The numbers added on the right of each figure show composition range. Lines and numbers on top of each figure are showing you P_H (bar) and T_S ($^{\circ}C$) samples experienced during measurement. Sudden intensity change at 8 h for Mg_xTi_{1-x} comes from electronics.

Intensities of 3 topmost curves (0.85 – 0.95 atom % Mg) are saturated at $P_H = 1$ bar. However, IR intensities for $x=0.44 - 0.70$ composition range show a secondary increase at $P_H = 5$ bar. This indicates that addition of Ni increases equilibrium hydrogen pressure of absorption. Those curves which have secondary increase of intensity also showed intensity drop (hydrogen desorption) at $P_H = 1 \times 10^{-6}$ bar and $T_S = 150$ $^{\circ}C$ (6 – 7 h). At $T_S = 200$ $^{\circ}C$ (7 – 10 h), the intensity drops for all compositions. These measurements indicate that for higher Ni concentrations dehydrogenation occurs at lower temperature 150 $^{\circ}C$, whereas for higher Mg concentrations - at 200 $^{\circ}C$. At 200 $^{\circ}C$ slope of the intensity decrease is higher for higher Mg concentrations, probably because hydrogen was not released for these concentrations at the preceding 150 $^{\circ}C$.

To study the effect of different microstructures on hydrogen absorption/desorption, the same set of experimental conditions was applied to the 250 $^{\circ}C$ -annealed Mg_xNi_{1-x} . Fig. 3(b) shows normalized IR intensity of the film. In general, the trend in intensity changes is similar to that of as-deposited Mg_xNi_{1-x} : intensity changes more rapidly for higher concentrations of Mg and the major intensity increase occurs at $P_H = 1$ bar (1 – 2 h). However, the significant difference between two Mg_xNi_{1-x} samples is that for the higher Mg concentrations IR intensity decreased with decrease of hydrogen pressure at 150 $^{\circ}C$ for the annealed film, as compared to 200 $^{\circ}C$ for the as-deposited film. These results suggest the lower desorption temperature for the annealed film. The differences may come from the differences in microstructures of as-deposited and annealed Mg_xNi_{1-x} , and points out on the importance of microstructural control.

The effect of different TM was explored by comparing hydrogenation of Mg_xNi_{1-x} and Mg_xTi_{1-x} films at the same conditions. Normalized IR intensity of Mg_xTi_{1-x} is shown on Fig. 3(c). For all the composition, intensity continued to increase both at $P_H = 1$ bar and 5 bar (1 – 4 h). Decrease in intensity occurred in two-step with removing of hydrogen pressure, at 150 $^{\circ}C$ and at 200 $^{\circ}C$ (6 – 10 h). As in the case of Mg_xNi_{1-x} samples, faster hydrogen absorption was observed for the higher Mg compositions. Compared with Mg_xNi_{1-x} samples, the slope of intensity change suggests slower hydrogen absorption rate for Mg_xTi_{1-x} , but faster hydrogen desorption. Intensity changes were not saturated at $P_H = 5$ bar, which indicates higher equilibrium pressure of absorption.

CONCLUSIONS

The IR emissivity imaging experiments with hydrogenation of $Mg_x(TM)_{1-x}$ composition spread films have convincingly demonstrated that the method is able to capture reaction of the films with hydrogen gas – increase of the intensity with adsorption and decrease with desorption. The method resolves different kinetics of hydrogenation for different compositions along a continuous compositional gradient of the films. Judging from the degree of IR intensity increase, the highest hydrogenation at 1 atm/150 °C occurs for higher Mg compositions ($0.9 > x > 0.75$), with desorption at 200 °C. This was observed for both MgNi and MgTi films and corresponds to the behavior of Mg phase. The method is also sensitive to minor microstructural differences, as it was shown for as-deposited and 250 °C post-annealed Mg_xNi_{1-x} . It was also shown that alloying with different TM elements clearly changes the hydrogen absorption/desorption behavior. According to the evolution of IR intensities, kinetics of hydrogenation for the Mg_xNi_{1-x} was comparable to that measured by optical and electrical resistivity methods by different research groups. However kinetics of hydrogenation for the Mg_xTi_{1-x} film is significantly slower to those reported in literature.

REFERENCES

1. DOE 2007 Annual Merit Review Proceedings Hydrogen Storage, http://www.hydrogen.energy.gov/annual_review07_storage.html
2. L. Schlapbach and A. Züttel, *Nature*, **414**, 353 (2001)
3. B. Dam, R. Gremaud, C. Broedersz, and R. Griessen, *Scripta Materialia*, **56** 853 (2007)
4. R. Gremaud, C.P. Broedersz, D.M. Borsa, A. Borgschulte, P. Mauron, H. Schreuders, J.H. Rector, B. Dam, and R. Griessen, *Adv. Mater.*, **19**, 2813 (2007)
5. C. H. Olk, G. G. Tibbetts, D. Simon, and J.J. Moleski, *J. Appl. Phys.*, **94**, 720 (2003)
6. G. Soloveichik, J. Lemmon, J. Cui, Y. Gao, T. Raber, J. Rijssenbeek, G. Rubinzstajn, and J.C. Zhao, DOE Presentation, (2007)
http://www1.eere.energy.gov/hydrogenandfuelcells/pdfs/ht_ge_soloveichik.pdf
7. L. Zaluski, A. Zaluska, P. Tessier, J. O. Stromolsen, and R. Schulz, *J. Alloys Comp.*, **217**, 295 (1995)
8. M. Dornheim, S. Doppiu, G. Barkhordarian, U. Boesenberg, T. Klassen, O. Gutfleisch and R. Bormann, *Scripta Materialia*, **56**, 841 (2007)
9. W. Lohstroh, R. J. Westerwaal, J. L. van Mechelen, C. Chacon, E. Johansson, B. Dam, and R. Griessen, *Phys. Rev. B*, **70**, 165411 (2004)
10. B. Farangis, P. Nachimuthu, T.J. Richardson, J. L. Slack, R.C.C. Perera, E.M. Gullikson, D. W. Lindle, and M. Rubin, *Phys. Rev. B*, **67**, 85106 (2003)
11. D.M. Borsa, R. Gremaud, A. Baldi, H. Schreuders, J.H. Rector, B. Kooi, P. Vermeulen, P.H.L. Notten, *Phys. Rev. B*, **75**, 205408 (2007)
12. S. Bao, K. Tajima, Y. Yamada, M. Okada, K. Yoshimura, *Applied Physics A: Materials Science & Processing*, **87**, 621 (2007)
13. J.L. Murray in *Binary Alloys Phase Diagrams*, Second Edition, Ed. T.B. Massalski, ASM International Materials Park, Ohio (1990), p. 2559